Article

Comparative Analysis of Active Bonded Piezoelectric Repair Systems for Damaged Structures under Mechanical and Thermo-Mechanical Loads

Mohammed Abdulla [1], Meftah Hrairi [1,*], Abdul Aabid [2,*], Nur Azam Abdullah [1] and Muneer Baig [2]

1   Department of Mechanical and Aerospace Engineering, Kulliyyah of Engineering, International Islamic
    University Malaysia, P.O. Box 10, Kuala Lumpur 50728, Malaysia; hafizabdulla2426@gmail.com (M.A.);
    azam@iium.edu.my (N.A.A.)
2   Department of Engineering Management, College of Engineering, Prince Sultan University,
    Riyadh P.O. Box 66833, Saudi Arabia; mbaig@psu.edu.sa
*   Correspondence: meftah@iium.edu.my (M.H.); aaabid@psu.edu.sa (A.A.)

Abstract: Active repair systems employing piezoelectric (PZT) patches have emerged as promising solutions for mitigating crack propagation and enhancing structural integrity in various engineering applications. However, the existing literature predominantly focuses on the application of PZT patches for repairing structures under mechanical loading. In this study, a finite element analysis (FEA) is employed to investigate the repair of a centre-cracked aluminium plate under both mechanical and thermo-mechanical loading conditions. This study explores the influence of key parameters, including temperature, PZT patch thickness, type of PZT material, adhesive material, and adhesive thickness, on the structural integrity and crack propagation behaviour. The results reveal significant differences in stress distribution and crack propagation tendencies under varying loading conditions and parameter settings. These findings emphasize the necessity of considering thermo-mechanical loading conditions and parameter variations when designing effective active repair systems. In conclusion, this study provides valuable insights into optimizing PZT patch-based repair strategies for improved structural integrity and crack mitigation in aerospace and other engineering applications under diverse loading scenarios.

Keywords: PZT; actuators; stress intensity factor; crack repair; plate

1. Introduction

In the ever-evolving fields of structural engineering and material science, the pursuit of resilient, adaptive methodologies to repair damaged or cracked structures remains a crucial and ongoing challenge. Piezoelectric actuators have emerged as a particularly promising solution, offering not only precise control but also efficient energy conversion, which is vital for effective structural repair [1]. Recent advancements in material science have paved the way for cutting-edge repair techniques that harness the unique properties of piezoelectric materials, enabling more sophisticated and responsive repair mechanisms that can adapt to dynamic stress conditions in real time [2,3]. However, understanding its behaviour under diverse environmental conditions is paramount. Repair techniques can be broadly classified into active and passive methods. Passive repair techniques involve static reinforcement without real-time adaptation to structural changes, whereas active repair methods can dynamically respond to evolving damage [4].

In fracture mechanics, significant attention is given to stress intensity factors (SIFs), which characterize the intense stress field at the tip of a crack. The fracture behaviour of a material is governed by the SIF, and a specimen is likely to fail when this factor reaches a critical threshold. In this study, the term active repair refers to the capability of PZT patches to dynamically adjust the stresses at the crack tip by applying controlled mechanical

stress through electrical actuation. While passive techniques do not adapt to real-time structural changes, the active approach involves applying an electrical voltage to the PZT patches, which generate controlled mechanical stress that counteracts the stresses at the crack tip. This dynamic adjustment enhances the structural integrity of the repaired plate by redistributing stresses around the crack area, leading to improved performance and longevity of the repair. The unique capability of piezoelectric materials to convert electrical energy into mechanical stress and vice versa enables their effective use in active repair systems [5]. This property allows PZT patches to provide real-time adjustments and control, contributing to better performance and durability of the repair. The electro-mechanical properties of the PZT materials have been employed for the control of delamination in beam structures [6,7]. Numerical simulations were performed to see the effect of repair under varying applied external voltage. A study on repair of a column, which was subjected to compressive load, was proposed in [8] with an aim to improve its load holding capacity. A crack on the cantilever structure subjected to alternate loading was repaired using a PZT patch and it was found to be effective for preventing the failure of the structure [9]. Duan et al. [10] performed a finite element analysis using commercial code ABAQUS for the restoration of a delaminated beam. The von Mises stress near the fracture point was effectively reduced with the assistance of an external electric field applied to the PZT patch.

For the repair of a delaminated structure, a numerical model was developed in [11], and the results of the same were validated by the finite element (FE) model. A decrease in the stress in the delamination region was observed using this repair methodology. An experiment was performed on a cantilever beam whose left end was fixed in all directions and on the other free end, an external load was applied, which was dynamic in nature. A crack on its centre on the top face was repaired by placing a PZT patch exactly on the same spot but on its bottom face [12]. An aluminium cracked panel was repaired using a PZT actuator using FE simulations and was validated further by conducting an experiment. Results showed that due to the activation of the PZT patch, a significant reduction in crack propagation was recorded [13]. Alaimo et al. [14] investigated the dynamic behaviour of piezoelectric active repair on cracked structures, focusing on the coupling between elastic and electric fields. Utilizing boundary element simulations, they incorporated a multidomain technique with an interface spring model to represent the crack and bonding layer. The analysis aimed to characterize the dynamic repairing mechanism by computing dynamic SIFs, emphasizing the influence of inertial forces on fracture mechanics behaviour. A study focused on the fracture behaviour of cracked structures, particularly the stress intensity factors near the fracture point, was conducted, which applied linear fracture mechanics to determine fracture toughness parameters of a cracked plate with a piezoelectric actuator under mode I load. An analytical model was developed to correlate piezoelectric parameters with the stress intensity factor and energy release rate [15]. Through three-dimensional finite element analyses, the effects of adhesive properties on the performance of active repairs in cracked aluminium plates under mode I loading were explored in [16].

Evaluation was based on the adhesive layer's shear modulus, with results indicating an inverse relationship between the shear modulus and stress intensity factor, serving as a fracture criterion. Abuzaid et al. [17] explored the effectiveness of PZT actuators in reducing crack damage propagation in thin plate structures, where they developed an analytical solution using the virtual crack closure technique, considering the singular stress at the fracture point and the coupling effects of the PZT patch. The analytical model's accuracy was validated against finite element simulations, showing good agreement. Results indicate that applying an extension mode of the PZT actuator reduces SIF. Abuzaid et al. [4] performed an experimental validation of the analytical model and FE analysis conducted using ANSYS 17.0 software, demonstrating results for mode I crack opening conditions. Furthermore, a parametric analysis investigated the influence and efficiency of piezoelectric actuators in mitigating SIF. The effectiveness of PZT actuators in reducing crack damage in engineering structures was investigated in a study [18]. It examined the active repair of centre-cracked

plates with these actuators by combining analytical and numerical methodologies. The weight functions approach was used to construct the analytical model, which then predicts the SIF caused by the actuators. Meanwhile, LEFM provided the solution for the plate under external loading. Fesharaki et al. [19] investigated piezoelectric actuator placement to mitigate stress concentration in classical plates under tensile force. They explored various plate configurations and employed a particle swarm optimization algorithm to identify optimal actuator locations based on stiffness ratios. Results indicated distinct placement models for stiffness ratios below and above 1, with actuators directly reducing stress for lower ratios and indirectly influencing stress distribution for higher ratios. Empirical tests validated the effectiveness of the proposed approach, offering insights for enhancing structural integrity through piezoelectric actuation in classical plates.

An FE method was used to model the composite plate with a crack. It utilized an eight-node structural shell element for the discretization of the composite material. On the other hand, an eight-node coupled-field element was used to model the piezoelectric patch to repair the cracked composite plate under both static and dynamic loading conditions [20]. The health of a multi-cracked beam was restored using PZT patches by the active repair technique. To analyze the repair performance of the same, Hai [21] used an analytical method and then validated it with the FE simulation method, which proved to be in good agreement. Asraar et al. [22] employed the machine learning technique for optimizing the SIF of the actively repaired aluminium plate using PZT patches. The important parameters of the host plate, patch, and adhesive were optimized using different ML models and the best models with high accuracy and the least error were highlighted. An investigation was conducted to study the impact of curing temperature of an adhesive on active repair using a mathematical model [23]. The principle of superposition and weight function method were utilized to analyze the effect of PZT patches for the repair of a C-type cracked specimen in [24]. Furthermore, a parametric study was performed to achieve the least SIF value. For a similar kind of repair using PZT patches, Aabid et al. [25] used the Design of Experiment (DOE) method for a similar type of repair using PZT patches in order to optimize the repair and achieve the minimum value of SIF using the optimal combination of input parameters. The results indicated that the DOE performed best in accomplishing its objective. Agrawal et al. [26] explored the optimal placement of piezoceramic actuators for controlling the shape of beam structures through both analytical and experimental approaches with an aim to identify the best locations and voltages for the actuators to minimize the discrepancy between the desired and achieved shapes of the beam. Kumar et al. [27] investigated active repair of a cracked cantilever beam under thermo-mechanical load; however, the results were found to be inconsistent due to uncertainty and irregular sensing behaviour of piezoelectric material. Voutetaki et al. [28] efficiently controlled the debonding process in dynamically loaded RC members strengthened with FRP sheets using PZT actuators/sensors and the EMI admittance concept in the active mode and extracted valuable results on optimum dynamic load to eliminate probable debonding failure. It was found that the optimal voltage level of the piezoelectric actuation eliminates the stress concentration at the debonding area of the FRP. Quantitatively, the normal tensile stresses at the critical concrete—FRP adhesive interface—are reduced below the concrete tensile strength, suggesting an effective FRP debonding prevention.

In aerospace applications, thermal variations due to altitude changes can induce stresses that interact with mechanical loads, potentially reducing the effectiveness of repairs over time [29]. The existing literature predominantly focuses on the application of PZT patches for repairing structures under mechanical loading, with limited attention given to thermo-mechanical loading, particularly in the context of cantilever structures. Additionally, the influence of various parameters under both mechanical and thermo-mechanical loading remains largely unexplored. To address this research gap, this study employs a finite element analysis to investigate the repair of centre-cracked aluminium 2024, a prevalent material in aerospace applications for fuselages and wings, under thermo-mechanical loading conditions. Furthermore, this study thoroughly examines key parameters related

to a PZT patch and adhesive properties that impact repair performance under both mechanical and thermo-mechanical loading. The analysis utilizes the commercial finite element software ANSYS 2022/R2 for comprehensive investigation.

2. Geometric Configuration of Plate

The specimen under investigation is a structural aluminium plate with the following dimensions: height H = 160 mm, width 2W = 100 mm, and thickness T = 1 mm. This plate features a centrally located crack with a length of 2a. The specimen is subjected to a uniform mechanical load of 1 MPa applied at both ends and a uniform thermal load ranging from −70 °C to 110 °C. To mitigate the effects of the crack, an actuation system comprising a PIC151 PZT actuator is employed. This actuator has dimensions of height H_p = 20 mm, width W_p = 40 mm, and thickness T_p = 0.5 mm. It is attached to the plate using an adhesive layer, which has dimensions of height H_{ad} = 20 mm, width W_{ad} = 40 mm, and thickness T_{ad} = 0.03 mm. The PZT patch is strategically positioned 1 mm away from the crack to optimize its effectiveness, as depicted in Figure 1.
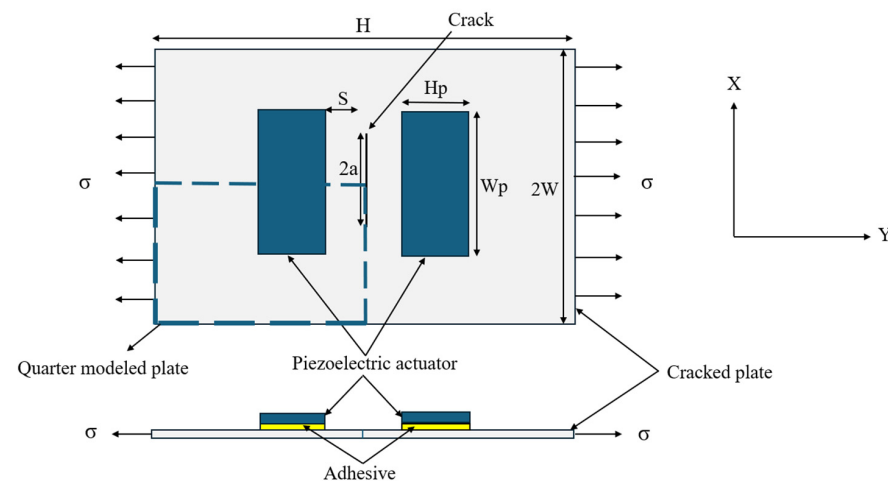

Figure 1. Piezoelectric patches bonded on centre-cracked plate using adhesive.

The choice of materials for the structural plate, PZT patch, and adhesive is critical for ensuring the durability and performance of the repaired specimen. The aluminium plate serves as the primary structural element, selected for its high strength-to-weight ratio, good thermal conductivity, and excellent corrosion resistance. These properties make aluminium a suitable material for structural applications subjected to both mechanical and thermal loads. The PIC151 PZT actuator is chosen for its high piezoelectric coefficients and electro-mechanical coupling factors, which enable efficient actuation. PZT (lead zirconate titanate) is a widely used piezoelectric material in actuators due to its ability to convert electrical energy into mechanical displacement. This property is harnessed to counteract the stress concentration around the crack, thereby enhancing the structural integrity of the plate. Table 1 details the material properties of the aluminium plate, and adhesives, while Table 2 lists the mechanical and thermal properties of PZT patches.

Table 1. Material properties of the plate and adhesives.

| Parameter | Host Plate | Adhesive | | |
		FM73	Araldite 2015	AV138/HV998
Density	2715 kg/m^3		1160 kg/m^3	
Poison's ratio	0.33	0.32	0.345	0.47
Young's modulus	68.95 GPa	1.83 GPa	5.1 GPa	4.59 GPa
Shear modulus		0.96 GPa	1.89 GPa	1.56 GPa
Thermal expansion coefficient (α)	22.5×10^{-6}/°C	50×10^{-6}/°C	85×10^{-6}/°C	67×10^{-6}/°C

Table 2. Material properties of PZT patches.

Parameter	PIC151 Patch	PZT-5H
Density	7800 kg/m^3	7870 kg/m^3
Compliance matrix	$S_{11} = 15.0 \times 10^{-12} \text{ m}^2/\text{N}$ $S_{33} = 19.0 \times 10^{-12} \text{ m}^2/\text{N}$	$S_{11} = 16.6 \times 10^{-12} \text{ m}^2/\text{N}$ $S_{33} = 21.0 \times 10^{-12} \text{ m}^2/\text{N}$
PZT strain coefficient	$d_{31} = -2.10 \times 10^{-10} \text{ m/V}$ $d_{32} = -2.10 \times 10^{-10} \text{ m/V}$	$d_{31} = -3.20 \times 10^{-10} \text{ m/V}$ $d_{32} = -3.20 \times 10^{-10} \text{ m/V}$
Piezoelectric stress coefficients	$e_{31} = -8.4746 \text{ C/m}^2$ $e_{33} = 21.231 \text{ C/m}^2$ $e_{15} = 14.8718 \text{ C/m}^2$	$e_{31} = -19.277 \text{ C/m}^2$ $e_{33} = 30.953 \text{ C/m}^2$ $e_{15} = 19.084 \text{ C/m}^2$
Thermal expansion coefficient (α)	$6 \times 10^{-6}/°\text{C}$ $6 \times 10^{-6}/°\text{C}$ $-5 \times 10^{-6}/°\text{C}$	$3.5 \times 10^{-6}/°\text{C}$ $3.5 \times 10^{-6}/°\text{C}$ $4 \times 10^{-6}/°\text{C}$

3. Active Repair Using Piezoelectric Actuators

Active repair using piezoelectric actuators leverages the electro-mechanical properties of PZT (lead zirconate titanate) patches to dynamically counteract stresses at the crack tip, thereby halting crack propagation. This innovative approach combines mechanical actuation and electrical control to enhance the durability of repaired structures.

In this study, we consider a centre-cracked plate subjected to external tensile loading, as shown in Figure 2. The tensile stress 'σ' is applied uniformly on the top and bottom edges of the plate, creating a stress concentration at the crack tip. To actively mitigate the crack's propagation, two PZT patches are placed: one directly above and the other below the crack. These patches are symmetrically positioned around the crack's plane, ensuring efficient stress counteraction.
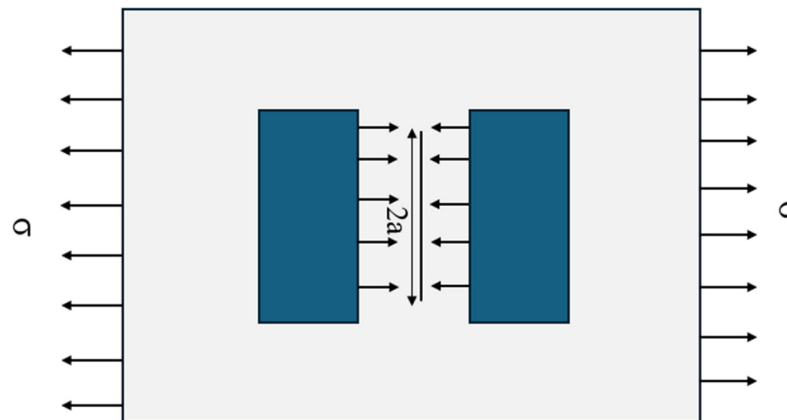
Figure 2. Active repair mechanism using PZT actuators.

3.1. Piezoelectric Effect and Its Application

The active repair mechanism relies on the converse piezoelectric effect, a characteristic of materials like PZT, enabling them to convert electrical energy into mechanical deformation. Piezoelectric materials exhibit two primary behaviours. The direct piezoelectric effect generates an electric charge in response to applied mechanical stress, as illustrated in Figure 3a, where the material deforms under an external mechanical force. In contrast, the converse piezoelectric effect, shown in Figure 3b, refers to the material's deformation (expansion or contraction) when exposed to an external electric field. This expansion or contraction occurs along its length L, with a change denoted as ΔL. This property is instrumental in active repair techniques, where controlled mechanical stress is applied through electrical actuation to adjust the stresses at the crack tip dynamically, enhancing the structural integrity of the repaired component [30].
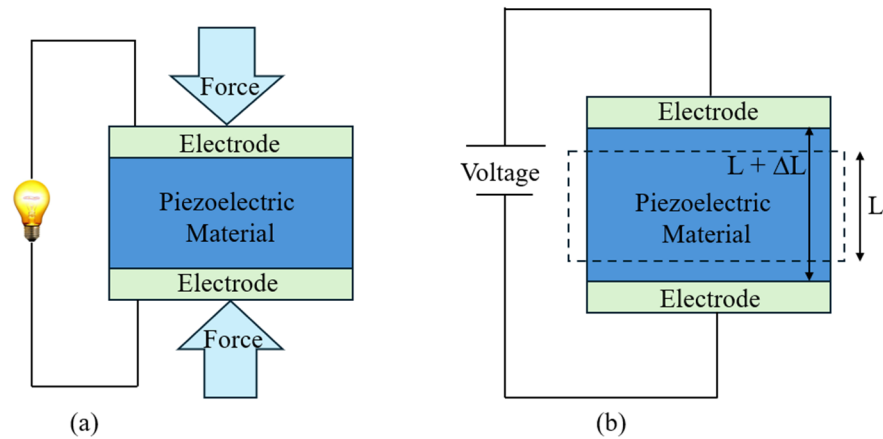
Figure 3. (**a**) Direct effect. (**b**) Converse effect of PZT material.

For the active repair strategy discussed here, the converse piezoelectric effect is exploited. When an electric voltage is applied across the PZT patches, they expand or contract depending on the polarity and magnitude of the applied voltage. In this case, both PZT patches are designed to expand upon voltage application, exerting controlled mechanical stress at the crack tip.

3.2. Mechanism of Crack Arrest through PZT Actuation

The application of a controlled electric voltage to the PZT patches induces expansion along their surfaces, generating compressive stresses at the crack tip. Since two PZT patches are placed on opposite sides of the crack, their simultaneous expansion applies a uniform compressive force at the crack plane. This compressive force opposes the external tensile stress σ, reducing the overall stress intensity near the crack tip.

4. Finite Element Method (FEM)

In the context of this study, the SIF is a critical parameter for understanding the fracture behaviour of materials under mechanical and thermo-mechanical loading. This section details the methodology used to calculate the SIF using FEM, focusing on the displacement extrapolation technique and the mathematical modelling involved.

4.1. Background of Modelling

In the finite element analysis, the stress and strain fields around the crack tip are calculated using the nodal displacements. The SIF can be determined by extrapolating these displacements. The process begins by solving the global stiffness matrix equation, Ku = F, where K is the stiffness matrix, u is the nodal displacement vector, and F is the force vector. The solution provides the nodal displacements, which are then used to calculate the stress and strain fields. At this point, it is important to note that the analysis follows the principles of Linear Elastic Fracture Mechanics (LEFM), which is a theoretical framework used to describe the behaviour of cracked structures. LEFM assumes that the material behaves elastically around the crack tip, with a very small plastic zone that can be neglected. The theory is particularly useful for determining the stress intensity factor (SIF), which quantifies the stress concentration at the crack tip. The SIF plays a crucial role in predicting the onset of crack growth under different loading conditions.

The stress functions developed by Westergaard [31] for a LEFM analysis are given by

$$\sigma_{xx} = \frac{K}{\sqrt{2\pi r}}\cos\frac{\theta}{2}\left[1 - \sin\frac{\theta}{2}\sin\frac{3\theta}{2}\right] \tag{1}$$

$$\sigma_{yy} = \frac{K}{\sqrt{2\pi r}}\cos\frac{\theta}{2}\left[1 + \sin\frac{\theta}{2}\sin\frac{3\theta}{2}\right] \tag{2}$$

$$\tau_{xy} = \frac{K}{\sqrt{2\pi r}}\cos\frac{\theta}{2}\sin\frac{\theta}{2}\cos\frac{3\theta}{2} \tag{3}$$

where r represents the radial distance from the crack tip to the point where the stress is being evaluated, measured in units of length, and θ is the angular coordinate measured from the crack plane expressed in radians and K is the stress intensity factor, expressed in MPa√m. These equations describe the normal and shear stresses near the crack tip. For validating these equations, LEFM assumes that the plastic zone at the crack tip is minimal.

4.2. Displacement Extrapolation Technique

The displacement extrapolation technique is a well-established method for calculating the SIF in linear elastic materials. This method relies on the high gradient of stress and strain fields around the crack tip. To accurately represent these fields, singular elements are employed as suggested in [32] and illustrated in Figure 4b. These elements, as suggested by Barsoum [33] and Henshell and Shaw [34], are designed to capture the $1/\sqrt{r}$ singularity of stresses and strains near the crack tip as shown in Figure 4a, while Figure 4c represents the singular element in 3D. In these elements, mid-side nodes are shifted to the quarter-point positions, significantly enhancing the accuracy of displacement and stress fields around the crack tip.
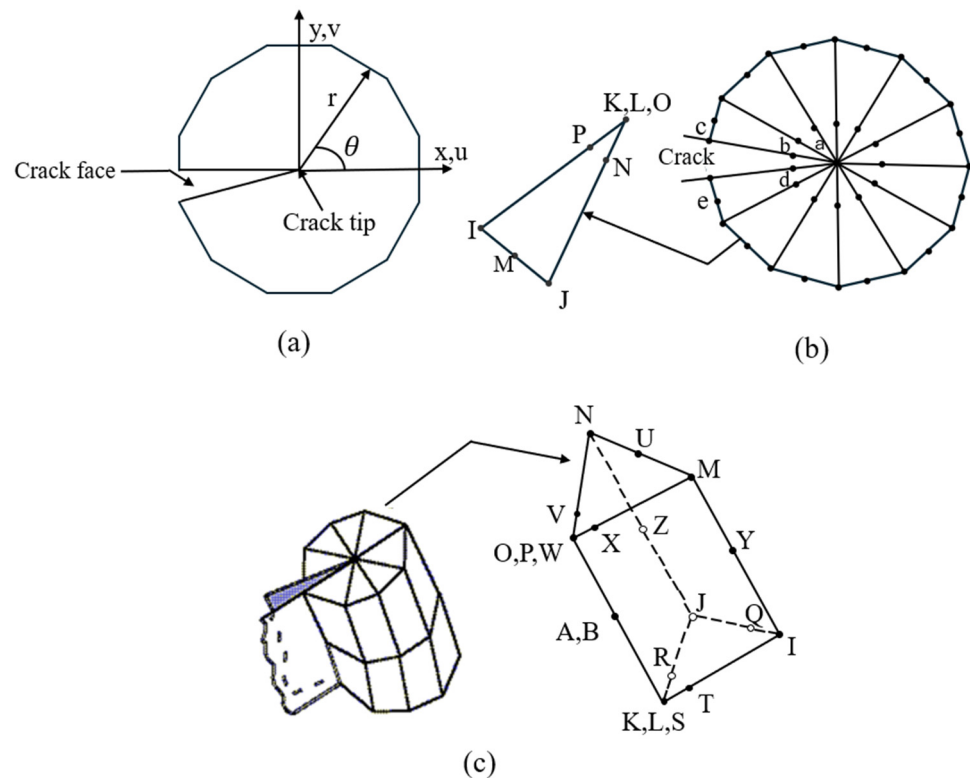

Figure 4. (**a**) Crack face and crack tip, (**b**) singular elements close to crack tip in 2D, (**c**) singular element in 3D.

4.3. Calculation of Stress Intensity Factor (SIF)

The SIF, K_I, that quantifies the stress state near the tip of a crack can be defined according to Tada et al. [35] as follows:

$$K_I = \sigma\sqrt{\pi a} \tag{4}$$

where σ represents the far-field applied stress and a is the crack length. This equation illustrates the influence of the applied stress and crack size on the SIF.

To calculate the SIF using the displacement extrapolation method, the following equation is used:

$$K_I = \sqrt{2\pi}\frac{2\mu}{1+k}\frac{|\Delta v|}{\sqrt{r}} \tag{5}$$

where Δv is the displacement of one crack face relative to the other, μ is the shear modulus, k is a dimensionless correction factor related to the geometric configuration of the crack, and r is the distance from the crack tip [36]. The term $\left(|\Delta v|/\sqrt{r}\right)$ is evaluated based on the displacements at three nodal points around the crack tip.

4.4. Nodal Displacement Extrapolation

To obtain the SIF, the displacements at nodes near the crack tip are analyzed. The value of v is normalized so that v at node I (where r = 0) is zero. The displacements at nodes J and K are used to determine parameters A and B such that

$$\frac{|\Delta v|}{\sqrt{r}} = A + B \cdot r \tag{6}$$

As r approaches zero, the expression simplifies to

$$\lim_{r \to 0}\frac{|\Delta v|}{\sqrt{r}} = A$$

Thus, the mode I SIF is calculated as

$$K_I = \sqrt{2\pi}\frac{2\mu A}{1+k} \tag{7}$$

4.5. Implementation in ANSYS

The software's KCALC command is used to compute the SIF based on the nodal displacements obtained from the FEM analysis. Singular elements are employed to accurately capture the displacement field near the crack tip. The displacement values from these elements are used in the extrapolation equations to calculate the SIF. This method ensures that the calculated SIF values are precise and reliable for assessing the fracture behaviour under mechanical and thermo-mechanical loading [37].

Thermal loading involves the application of temperature variations that induce thermal stresses within a material due to expansion or contraction. For an aluminium plate with a crack, the thermal stresses can be described by the following governing equations:

The thermal stress $\sigma_{thermal}$ in an isotropic material can be expressed as mentioned in Equation (8) [38]:

$$\sigma_{thermal} = E\alpha\Delta T \tag{8}$$

where E is the Young's modulus, α is the coefficient of thermal expansion, and ΔT is the change in temperature.

When considering the combined mechanical and thermal loading, the total stress at a point is the sum of the mechanical and thermal stress:

$$\sigma_{total} = \sigma_{mechanical} + \sigma_{thermal} \tag{9}$$

Therefore, the stress intensity factor at the crack tip under thermo-mechanical loading can be expressed as the sum of the stress intensity factors due to mechanical and thermal loading:

$$K_{I(total)} = K_{I(mechanical)} + K_{I(thermal)} \tag{10}$$

The energy release rate G, which measures the energy available for crack propagation per unit crack growth, is a crucial parameter in fracture mechanics [39]. For mode I loading, it can be defined as

$$G = \frac{K_{I(total)}^2}{E} \tag{11}$$

4.6. Structural Modelling and Meshing

Using a coupled-field analysis approach, this study examines the interactive behaviour of structural and electric fields, with a specific focus on piezoelectric effects. The piezoelectric actuator is represented by the coupled element SOLID226, which consists of 20 nodes and supports up to five degrees of freedom. SOLID226 empowers engineers to navigate the complexities of electro-mechanical interactions with precision. For a visual representation, refer to Figure 5 illustrating the schematic view of the SOLID226 element as depicted in the ANSYS Mechanical APDL Theory Reference [40].
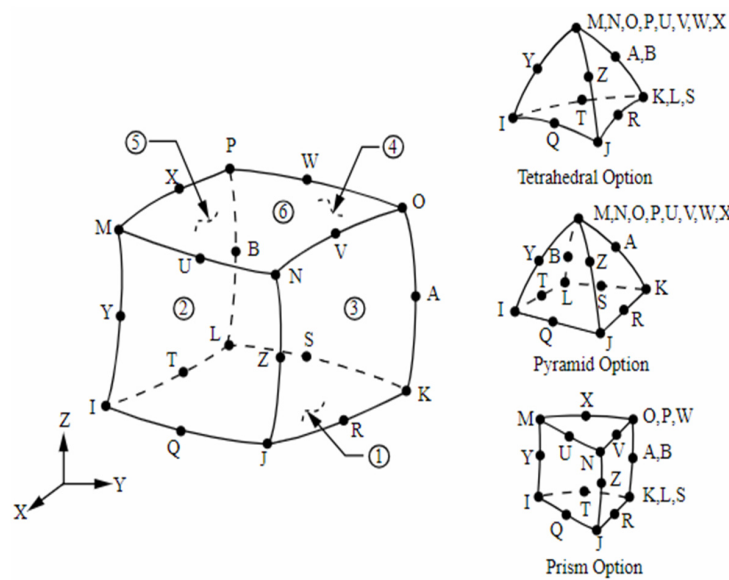
Figure 5. SOLID226 coupled-field element [40].

To simulate the cracked plate and the adhesive layer between the plate and the patch, we used the SOLID186 element. The SOLID186 is a three-dimensional solid element, shown in Figure 6, which features higher-order characteristics with quadratic displacement behaviour. This element has 20 nodes, each with three degrees of freedom, including translations in the x, y, and z directions. It is specifically designed for a solid structure analysis and is highly effective in linear applications because of its advanced capabilities. SOLID186 provides excellent precision and accuracy in modelling complex structural behaviours, making it an ideal choice for scenarios that require a detailed simulation of intricate component interactions.
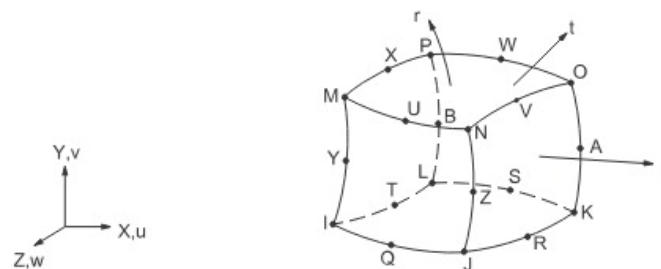

Figure 6. SOLID186 element [40].

To optimize computation efficiency and reduce processing requirements, the plate is modelled using only one-quarter of its geometry, taking advantage of symmetry as shown in Figure 1. Additionally, a fine mesh is implemented around the crack front to accurately compute the SIF. SIF is determined by employing the interaction integral method, which incorporates the virtual crack extension technique. This method yields precise results while reducing the required mesh density. Stress and strain singularities are created around the crack tip using singular elements aligned with the crack direction. Figure 7 depicts the comprehensive finite element models for the quarter model. The crack front consists of ten singular elements, and the PZT actuator is comprised of 5000 coupled-field elements. The damaged plate is modelled using 15,146 high-order reduced integration solid elements, while the adhesive layer is represented by 2500 high-order reduced integration solid elements. This modelling approach guarantees a precise simulation of the piezoelectric actuator's interaction with the structural plate.
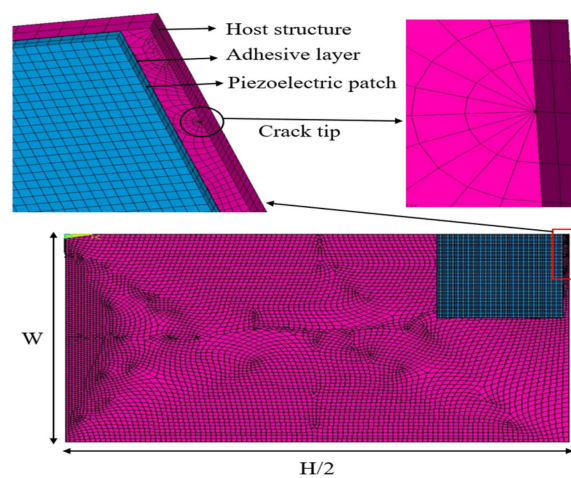

Figure 7. Meshed model of plate.

Figure 8 illustrates the boundary conditions and external loading applied to the geometric model. The model represents the right bottom quarter of the cracked plate for symmetrical considerations, reducing computational complexity without compromising accuracy. The boundary conditions, clearly marked in the figure, show fixed constraints along the symmetry lines with external tensile loading applied perpendicularly.
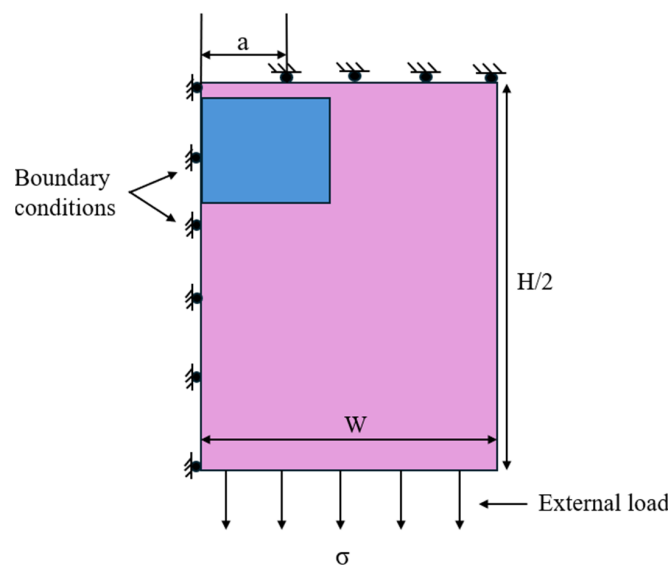

Figure 8. Boundary conditions and external tensile loading.

A constant temperature of between $-70°$ C and $110\,°$C was applied to the entire model in addition to an external mechanical stress. As a result, the model's volumes all reach the same temperatures. The model is shown in Figure 9 with a constant temperature of $110\,°$C.
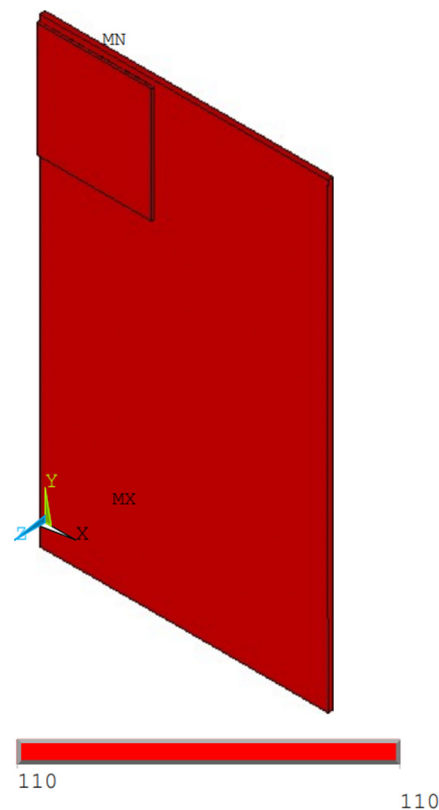

Figure 9. Temperature applied to model.

4.7. Mesh Convergence Test

In this study, mesh sensitivity tests were conducted to evaluate the accuracy and computational efficiency of different mesh types for the active repair of a cracked plate using PZT actuators under mechanical and thermo-mechanical loading conditions. The tests were divided into two sections: one focusing on mechanical loading with a mechanical load of 1 MPa and the other on thermo-mechanical loading where the model was subjected to a temperature of $110\,°$C along with a tensile mechanical load of 1 MPa. For meshing the patch and adhesive, a structured mesh was used, while an unstructured mesh was applied to the plate, with each boundary line of the plate divided into several elements. The meshing focused particularly on the crack tip area, where singular elements were employed to capture the stress concentration accurately. The crack tip was discretized into 6, 10, and 16 circumferential elements for the coarse, intermediate, and fine meshes, respectively, ensuring an increasingly refined analysis of the stress intensity factor. The element sizes for the PZT patch and adhesive were 0.0008m, 0.0005m, and 0.0002m for these respective meshes. The results and the rationale for selecting the intermediate mesh type are discussed below.

Under pure mechanical loading conditions, the coarse mesh configuration required the least computational time but exhibited the highest error in the SIF value, with a percentage difference of 9% compared to the fine mesh as depicted in Figure 10. The intermediate mesh provided a good balance between accuracy and computational efficiency, with a percentage difference in SIF of 3.2% compared to the fine mesh. This intermediate mesh took significantly less time to solve the problem, being less than half the computational time of the fine mesh. While the fine mesh yielded the most accurate SIF values, it required more than double the computational time compared to the intermediate mesh. The details

of the mesh analysis and the number of elements used in this study have been listed in Table 3.
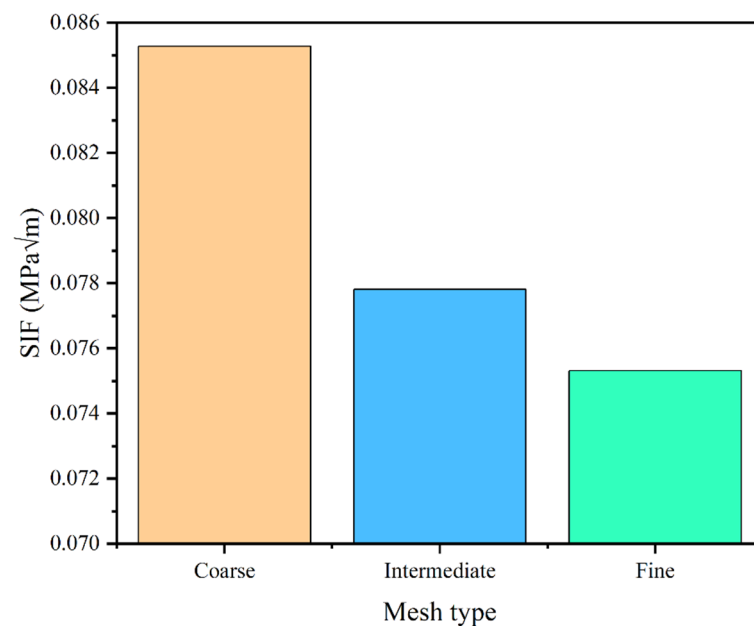

Figure 10. Mesh sensitivity test under mechanical loading.

Table 3. Mesh analysis under mechanical loading.

Mesh Type	No. of Elements	No. of Nodes	CPU Runtime	SIF
Coarse	8708	15,231	368 s	0.05828
Intermediate	27,114	51,649	757 s	0.07781
Fine	54,927	98,651	1593 s	0.07531

For thermo-mechanical loading conditions, the coarse mesh again required the least computational time but had the highest error in SIF values, with a percentage difference of 13% compared to the fine mesh as illustrated in Figure 11. The intermediate mesh continued to provide a balance between accuracy and computational efficiency, with a percentage difference in SIF of 4.5% compared to the fine mesh and nearly half the computational time of the fine mesh. Although the fine mesh provided the most accurate SIF values, it demanded significantly more computational time, more than double that of the intermediate mesh. The computational time for solving thermo-mechanical loading problems was higher than for mechanical loading alone, due to the added complexity of modelling thermal stresses and their interactions with mechanical stresses. The selection of mesh configurations was based on a balance between computational time and accuracy in predicting the SIF. Coarse meshes, while requiring the least computational time, resulted in greater error in SIF calculations. Fine meshes, though the most accurate, required substantially more computational time. The intermediate mesh, with a reasonable element size, was chosen under both mechanical and thermo-mechanical loading for its ability to reduce SIF error while maintaining computational efficiency, thus providing the best compromise between accuracy and time consumption. The details of the mesh analysis under thermo-mechanical loading have been listed in Table 4.
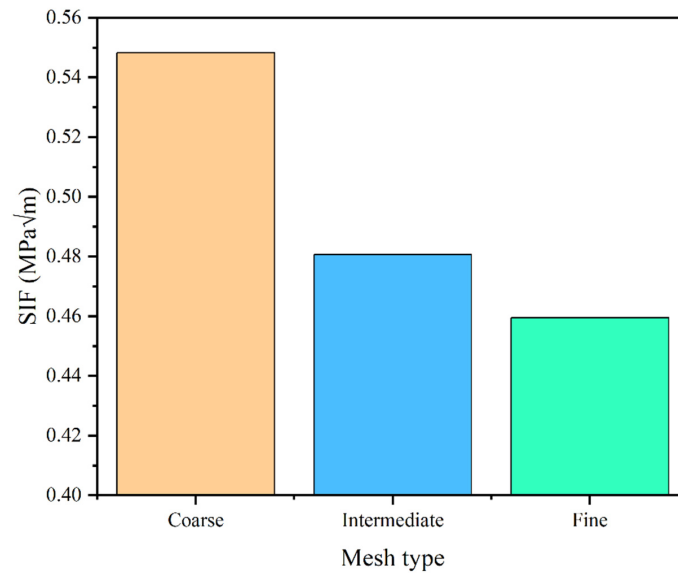
Figure 11. Mesh sensitivity test under thermo-mechanical loading.

Table 4. Mesh analysis under thermo-mechanical loading.

Mesh Type	No. of Elements	No. of Nodes	CPU Runtime	SIF
Coarse	9983	16,958	624 s	0.54823
Intermediate	26,418	48,214	1179 s	0.48068
Fine	59,715	102,564	2685 s	0.4595

4.8. Validation of Present Work

4.8.1. Validation of Unrepaired Plate

The present work has been verified using theoretical and experimental existing work. To obtain the SIF value, one needs to define a path and must ensure that the crack face is aligned parallel to the x-axis to establish a local coordinate system for the crack tip, with the y-axis perpendicular to the crack face. The SIF was then computed using the KCALC command in ANSYS. The SIF obtained for the unrepaired plate was verified using Equation (4) by Tada et al. [35]. The results of both the literature and the present work showed good agreement with less error as can be seen in Figure 12 and Table 5.
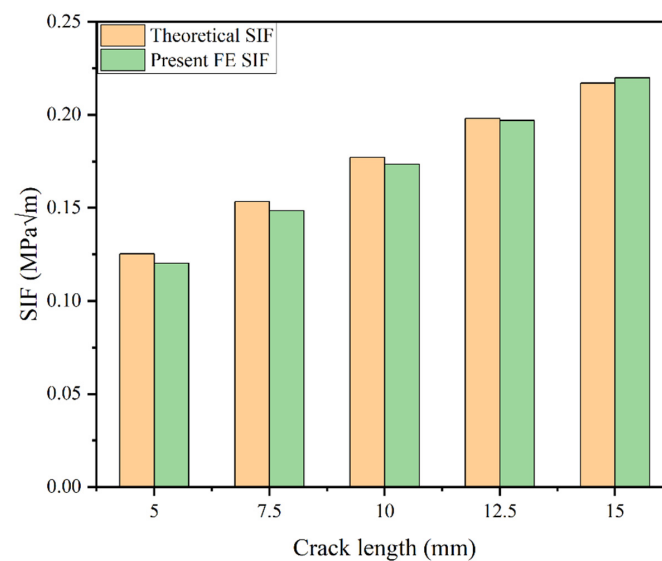

Figure 12. Theoretical vs. finite element results of SIF.

Table 5. Verification of present results.

Case	Type	SIF	Percentage Error
Abuzaid et al. [4]	Experimental	1.01335	3.62%
Current work	FE Simulation	1.0514	

4.8.2. Validation of Repaired Plate Using Active Repair

To verify the results, the displacements derived from the analytical method are compared with those obtained from the finite element (FE) analysis for a PIC151 piezoelectric actuator from PI Ceramic, which operates in the extension mode (d_{31}) under an applied voltage of 100 V. The constitutive equations of the piezoelectric material are outlined as follows:

$$S_1 = s_{11}^E T_1 + d_{31} E_3 \tag{12}$$

$$D_3 = d_{31} T_1 + \varepsilon_{33}^T E_3 \tag{13}$$

When the external mechanical load is not considered, the strain in the free actuator is

$$S_1 = d_{31} E_3 \tag{14}$$

$$\delta_o = S_1 I_p \tag{15}$$

$$E_3 = V/t_p \tag{16}$$

where S_1 represents the mechanical strain, T_1 denotes the stress, D_3 indicates the electrical displacement, E_3 stands for the electric field, s_{11}^E is the mechanical compliance at the zero electric field, ε_{33}^T is the dielectric constant at zero stress, d_{31} is the piezoelectric coefficient, δ_o is the displacement, and I_p and t_p are the length and thickness of the piezoelectric material, respectively.

The actuator has dimensions of t_p = 0.3 mm for thickness and I_p = 20 mm for length. Due to symmetry, only one-fourth of the piezoelectric patch is modelled. Nodes along the x-plane interface were constrained in the x-direction, while nodes along the y-plane interface were constrained in the y-direction. The FE displacement result, δ_{oF} = −1.435 μm, is in good agreement with the analytical result, δ_o = −1.40 μm. Furthermore, an experimental study performed by Abuzaid et al. [4] on the repair of edge-cracked aluminium plates using PIC 151 actuators was referenced. The actuators were bonded around the crack region with an Araldite 2015 adhesive. The host specimen dimensions were 220 mm in height, 38.5 mm in width, and 1 mm in thickness. To determine the stress intensity factor (SIF) at the fracture tip, electric resistance strain gauges were employed. The PZT actuators were activated by an electric field of 100 V using an E-413 piezo amplifier (Karlsruhe, Germany).

5. Results and Discussion

5.1. Mechanical Load

Under pure mechanical loading, the PZT patches significantly reduced the SIF at the crack tip. The effectiveness of the active repair is quantified by the reduction in SIF. The SIF reduction indicates the ability of the PZT actuators to stabilize the crack and prevent its further propagation. For a smaller crack length (5 mm) repaired using PIC151, the PZT actuators are highly effective, achieving a 37.26% reduction in SIF. This significant drop demonstrates the strong influence of the induced compressive stresses in mitigating the crack growth. However, as the crack length increases, the effectiveness of the active repair diminishes. Specifically, the SIF reduction for a 7.5 mm crack is 35.83%; for a 10 mm crack, it is 32.02%; for a 12.5 mm crack, it is 30.44%; and for a 15 mm crack, it is 28.25%, as can be seen from Figure 13. This trend can be attributed to the larger crack surface area and the increased stress concentration at the crack tip as the crack lengthens. The compressive stress generated by the PZT patches becomes less effective in counteracting the higher tensile stresses present in longer cracks.
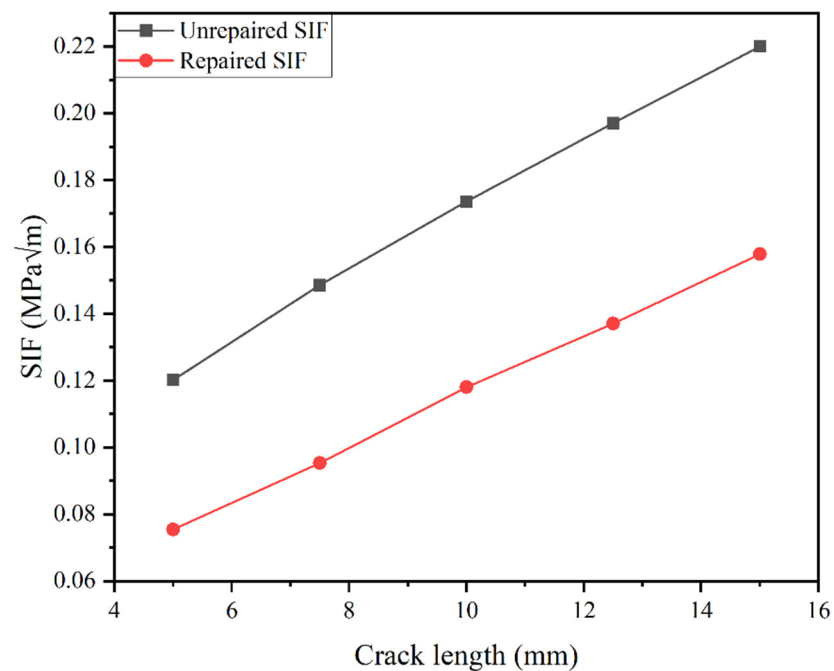
Figure 13. SIF for different crack length.

5.2. Effect of PZT Patch Thickness

In this section, the impact of varying the PZT patch thickness under different voltage levels was examined, as illustrated in Figure 14. For a crack of 10 mm actuated by a PIC151 patch, the results reveal that the normalized SIF reduction exhibits a slight increase as the thickness of the piezoelectric actuators increases in passive and low-voltage conditions. This indicates that thicker piezoelectric actuators are somewhat more effective in reducing SIF under these circumstances. However, this trend does not hold consistently as the applied electric field intensifies. When the electric field is relatively high, the impact of increasing the actuator thickness diminishes and can even reverse. Specifically, at these higher voltage levels, thicker piezoelectric actuators become less effective, leading to an increase in SIF compared to thinner actuators. This phenomenon can be explained by the behaviour of strain produced by the piezoelectric actuators. At low voltages, thicker actuators can better distribute and counteract the stress concentration around the crack due to their larger volume and mechanical stiffness. This results in a reduction in SIF. However, as the voltage increases, the relationship between actuator thickness and strain becomes more complex. Thicker actuators may reach a point where their ability to generate effective strain diminishes. This could be due to nonlinear piezoelectric effects and material saturation, where the efficiency of strain production decreases and internal stresses increase, counteracting the benefits observed at lower voltages. In summary, while thicker piezoelectric actuators initially provide better SIF reduction in low-voltage scenarios, their effectiveness decreases and reverses at higher voltages due to changes in strain behaviour and the onset of nonlinear material properties.

5.3. Effect of Different PZT Materials

In our study comparing the effectiveness of PZT materials, namely PZT-5H and PIC151, for active repair under mechanical loading conditions, we observed compelling results as shown in Figure 15. The superior performance of PZT-5H in reducing the SIF compared to PIC151 can be attributed to several key factors. Firstly, PZT-5H exhibits higher piezoelectric coefficients compared to PIC151. With higher values for $e31$, $e33$, and $e15$, PZT-5H can generate larger electric fields when subjected to an applied voltage. Consequently, this results in the induction of more significant mechanical stresses, which effectively counteract stress concentrations at the crack tip. In contrast, the lower piezoelectric coefficients of

PIC151 limit its ability to induce comparable stresses, leading to a less effective reduction in SIF. Secondly, the lower stiffness coefficients of PZT-5H play a crucial role in its superior performance. With lower values of stiffness coefficients, PZT-5H deforms more readily under the same applied voltage compared to PIC151. This enhanced flexibility allows PZT-5H to transfer induced stresses more effectively to the surrounding material, facilitating better stress distribution and a more efficient reduction in SIF around the crack tip. The combined effect of these factors makes PZT-5H significantly more effective for active repair applications. Its ability to generate higher induced stresses and distribute them more efficiently results in a greater reduction in SIF compared to PIC151. In conclusion, the combination of higher piezoelectric coefficients and lower stiffness makes PZT-5H a more effective material for active repair applications. Its ability to induce larger stresses and distribute them more efficiently leads to a significantly lower SIF, highlighting the superior performance of PZT-5H in enhancing the durability and reliability of repaired structures.
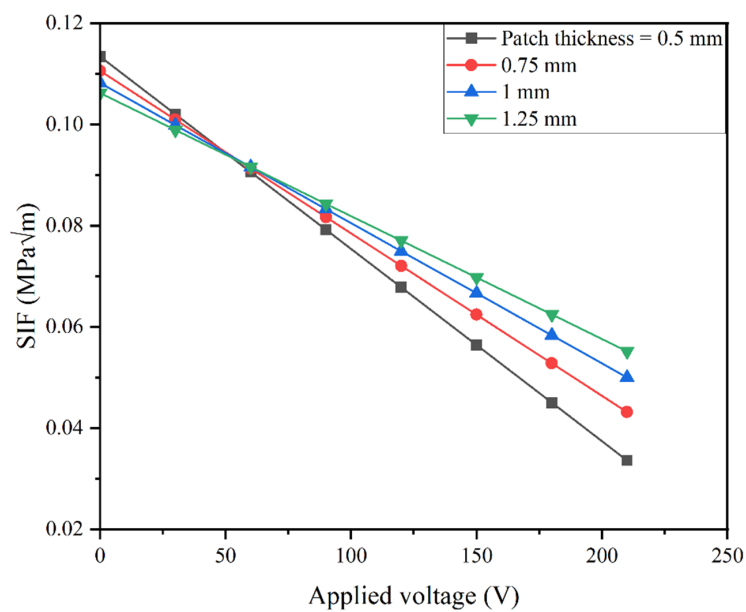

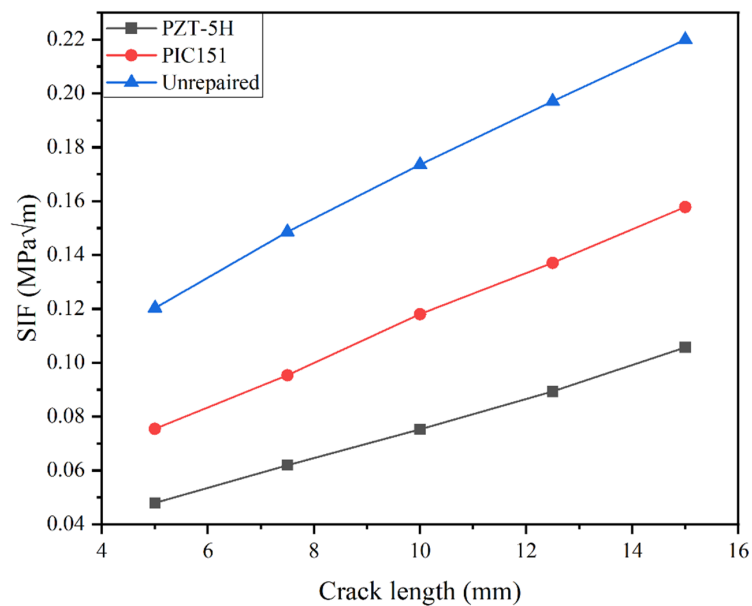**Figure 14.** SIF for PZT patch thicknesses under mechanical loading.

Figure 15. SIF for different PZT materials under mechanical loading.

5.4. Effect of Different Adhesive Material

In this study, three different adhesives were tested for their effectiveness in active repair under mechanical loading conditions for different crack lengths. The adhesives used were Araldite 2015, AV138/HV998, and FM73, each with distinct mechanical properties where the actuator employed was PIC151. Araldite 2015 demonstrated the most effective performance, yielding the lowest SIF. Following this, AV138 showed moderate effectiveness. Finally, FM73 resulted in the highest SIF among the three adhesives tested. The results indicate that the mechanical properties of the adhesives play a crucial role in their performance in active repair applications. Araldite 2015's higher Young's modulus and shear modulus suggest a stiffer and more robust material capable of better stress distribution and mitigation around the crack, thus leading to the lowest SIF. In contrast, FM73's significantly lower Young's modulus and shear modulus imply a less stiff adhesive, which is less effective at reducing stress concentrations, resulting in the highest SIF. AV138/HV998, with intermediate properties, performed correspondingly, achieving SIF values between the other two adhesives as can be seen in Figure 16.
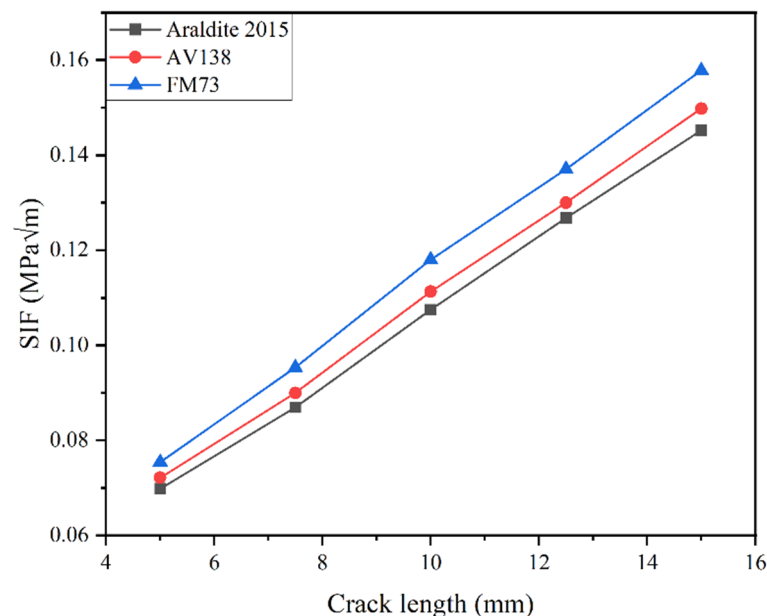

Figure 16. SIF for different adhesive materials under mechanical loading.

5.5. Effect of Adhesive Thickness

For a crack of 10 mm in an aluminium plate repaired using a PIC151 actuator actuated by 100V, it was found that as adhesive thickness increased under mechanical loading, the SIF also increased as can be seen from Figure 17. The explanation for this phenomenon is that although a thicker layer of an adhesive can improve adhesion strength, it also has the tendency to diffuse stresses transferred to the plate from the patch generated due to actuation. This dissipation reduces the efficiency of the compressive stress transfer, which lessens the patch's positive effects. Consequently, there is an ineffective reduction in the stress concentration at the crack tip, leading to an increase in SIF. Therefore, even though thicker adhesives offer improved adhesion, they must be optimized to ensure efficient load transmission and stress distribution to maintain structural integrity under mechanical loading conditions.

5.6. Effect of Increasing Applied Voltage

In the study of active repair using PZT patches under mechanical loading, the effect of increasing the applied voltage on the PZT patches was investigated. For a crack of 10 mm restored using a PIC151 actuator, the results demonstrated a significant reduction in the SIF with increasing applied voltage. Specifically, an impressive 46% reduction in SIF

was observed when the voltage was increased from 0 V to 140 V as depicted in Figure 18. This significant decrease in SIF can be attributed to the piezoelectric properties of the PZT patches. The higher the applied voltage, the greater the induced mechanical strain and, consequently, the greater the compressive stresses generated by the PZT patches. As a result, the tensile stresses at the crack tip are effectively reduced, leading to a lower SIF. The induced compressive stresses help to stabilize the crack and prevent its further propagation, enhancing the integrity and durability of the repaired structure. The efficiency of the PZT patches in mitigating crack growth is directly proportional to the voltage applied, as higher voltages result in stronger piezoelectric responses and more substantial compressive stress generation.
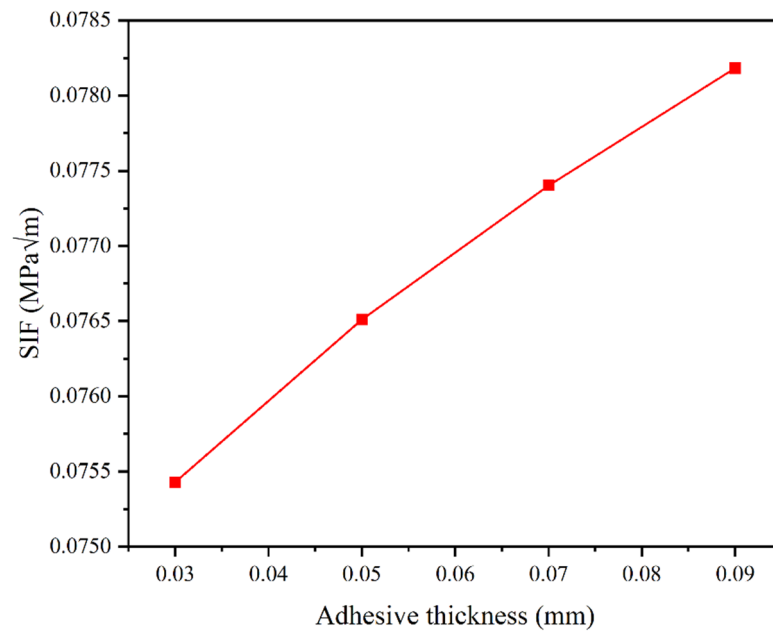

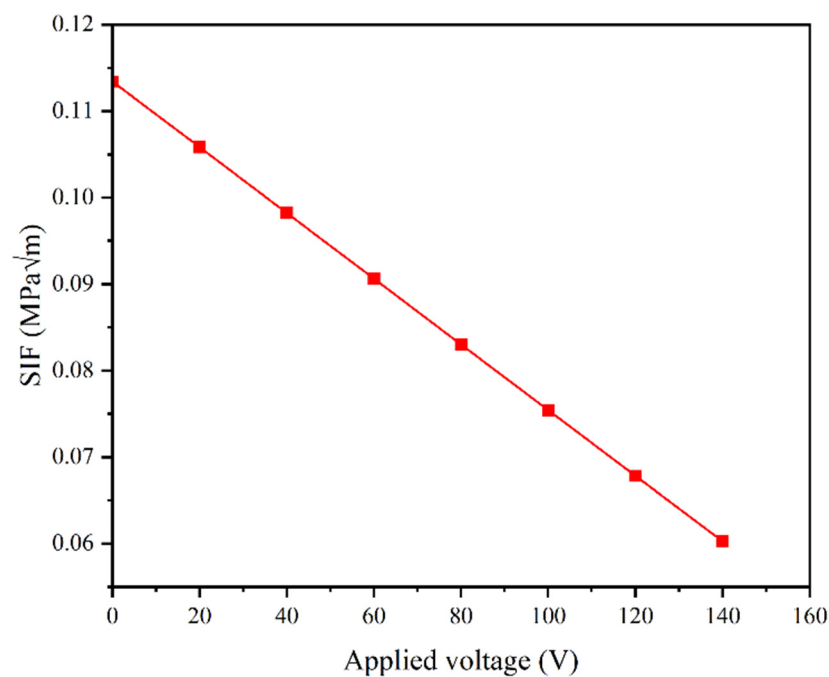**Figure 17.** SIF for adhesive thicknesses under mechanical loading.

Figure 18. SIF for increasing applied voltage under mechanical loading.

5.7. Thermo-Mechanical Load

5.7.1. Effect of Positive Temperature

Under the application of uniform positive temperatures to the entire model, which includes the PZT patch, the host plate, and the adhesive, significant increases in the SIF were observed across all crack lengths. This observation is illustrated in Figure 19 where the x-axis represents the temperature, and the y-axis represents the SIF. As temperature increases, both the PZT patch and the host plate experience thermal expansion, but due to their differing coefficients of thermal expansion (CTE), the induced thermal stresses vary significantly. The PZT patch has a CTE of $6 \times 10^{-6}/°C$ in the x- and y-directions and $-5 \times 10^{-6}/°C$ in the z-direction, meaning it expands slightly in-plane but contracts through its thickness as temperature rises. In contrast, the host plate has a higher CTE of $22.5 \times 10^{-6}/°C$ in all directions, resulting in more substantial expansion compared to the PZT patch. The adhesive, with a CTE of $50 \times 10^{-6}/°C$, expands even more significantly. At higher temperatures, such as 90 °C and 110 °C, these differential expansions between the PZT patch, the host plate, and the adhesive create substantial thermal stresses, which exacerbate the stress concentration at the crack tip. This is particularly evident for longer crack lengths where the stress intensity becomes more pronounced due to the larger surface area of the crack exposed to these thermal stresses. Consequently, the SIF increases significantly with both the temperature rise and the increase in crack length.
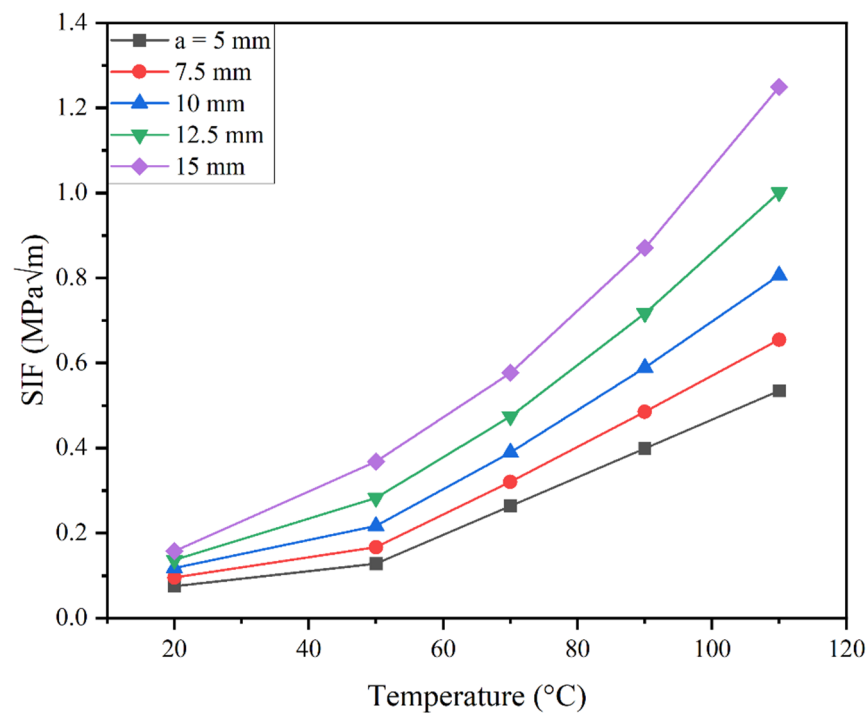

Figure 19. SIF for positive temperatures.

The thermal mismatch leads to increased tensile stresses in the vicinity of the crack tip, overwhelming the compressive stresses generated by the PZT actuators. At elevated temperatures, the effectiveness of the PZT patches to mitigate crack propagation diminishes because the thermal expansion-induced tensile stresses dominate, thereby increasing the SIF. This effect is compounded in longer cracks, where the stress intensity is naturally higher, leading to a much more pronounced increase in SIF at higher temperatures. In summary, the combined effect of a temperature rise and differing thermal expansion properties of the materials used in the repair system results in significantly higher SIF values. This increase is particularly dramatic at higher temperatures and for longer cracks, highlighting the challenges of maintaining effective crack mitigation under thermo-mechanical loading conditions.

5.7.2. Effect of Negative Temperature

During cooling under negative temperature, the aluminium plate, with its higher coefficient of thermal expansion (CTE) of $22.5 \times 10^{-6}/°C$, undergoes more significant contraction compared to the surrounding PZT patches, which have a CTE of $6 \times 10^{-6}/°C$. The adhesive, with an even higher CTE of $50 \times 10^{-6}/°C$, contracts the most. This differential contraction introduces a complex interplay of forces within the structure. The PZT patches, due to their lower CTE values, contract less during the cooling process. This difference creates a scenario where the PZT patches act as restraining forces on the contracting aluminium plate. This interaction results in tensile stresses in the aluminium plate near the crack tip. As the temperature drops further, these thermal mismatch-induced tensile stresses become more pronounced, especially for longer cracks, which naturally have higher stress intensities. The PZT patches, originally intended to mitigate crack propagation through the generation of compressive stresses, become less effective under these conditions. The tensile stresses induced by the differential thermal contraction overshadow the compressive stresses, leading to an increase in the SIF as depicted in Figure 20.
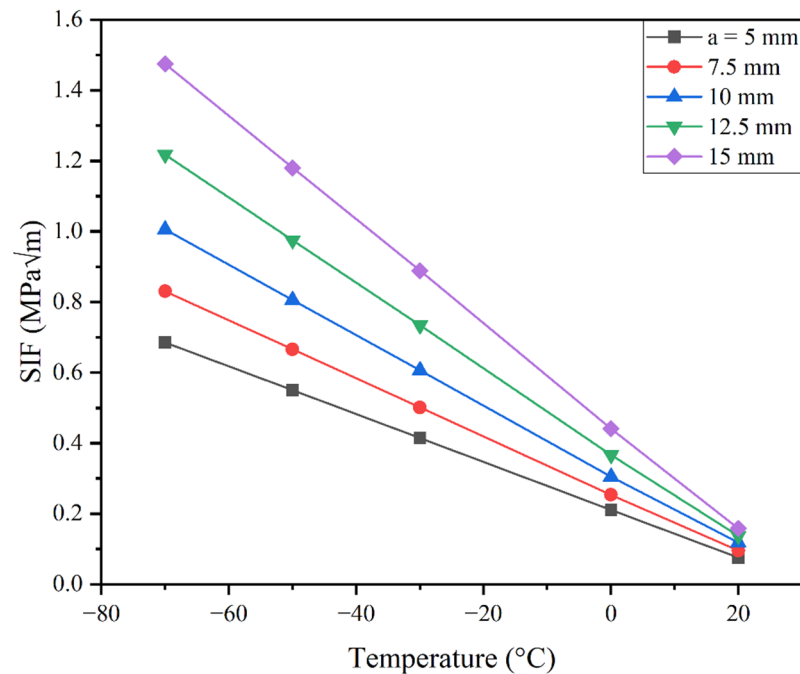

Figure 20. SIF for negative temperatures.

5.7.3. Effect of PZT Patch Thickness

For a 10 mm crack, the influence of PZT patch thickness was analyzed under thermomechanical loading. The PZT patches significantly impact the SIF at the crack tip in such conditions. The PZT patches have a negative coefficient of thermal expansion (CTE) of $-5 \times 10^{-6}/°C$ in the z-direction, which means that they contract when exposed to increased temperatures. As the thickness of the PZT patch increases, this contraction effect becomes more pronounced, providing greater compressive forces that help to counteract the tensile stresses caused by the thermal expansion of the surrounding materials. The aluminium plate, with a higher CTE of $22.5 \times 10^{-6}/°C$, expands significantly more than the PZT patches when the temperature rises. The adhesive, with an even higher CTE of $50 \times 10^{-6}/°C$, expands the most among the materials. This differential expansion creates complex thermal stresses within the structure. The thicker PZT patches, by contracting more significantly in the z-direction due to their increased volume, generate higher compressive stresses. These stresses effectively counteract the tensile stresses induced by the expansion of the aluminium plate and adhesive. The increased thickness of the PZT patches thus enhances their ability to mitigate the tensile stresses around the crack tip, leading to a

reduction in the SIF. As a result, thicker PZT patches provide a more stable and balanced stress distribution, effectively reducing the likelihood of crack propagation under thermo-mechanical loading as shown in Figure 21.
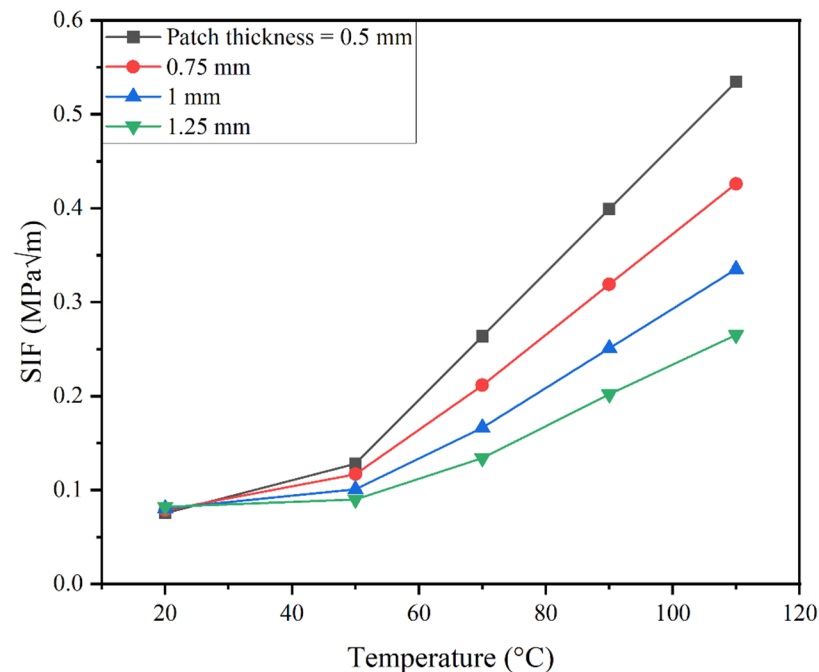

Figure 21. SIF for PZT patch thicknesses under thermo-mechanical loading.

5.7.4. Effect of Different PZT Materials

Under thermo-mechanical loading conditions for a crack of 10 mm, the analysis revealed that PZT-5H resulted in a lower SIF compared to PIC151 as illustrated in Figure 22. Specifically, while both materials experienced an increase in SIF with rising temperatures, PZT-5H consistently showed a lower SIF value. This outcome can be attributed to several key material properties and their interactions under combined thermal and mechanical stresses. PZT-5H has a lower coefficient of thermal expansion compared to PIC151. The lower CTE of PZT-5H means that it undergoes less thermal expansion under temperature changes, which helps reduce thermal stresses around the crack tip. Additionally, the stiffness properties of PZT-5H allow it to deform more easily and distribute stresses more effectively, reducing stress concentrations. Furthermore, the piezoelectric properties of PZT-5H, with higher piezoelectric coefficients, enable it to generate larger induced stresses under an applied electric field, contributing to the mitigation of crack propagation. These factors combined suggest that PZT-5H's superior thermo-mechanical behaviour, characterized by less thermal expansion and more effective stress distribution, leads to a lower SIF value compared to PIC151 under the same loading conditions.

5.7.5. Effect of Different Adhesive Material

In the same study conducted to evaluate the effectiveness of different adhesives in active repair under thermo-mechanical loading conditions, three adhesives were tested: Araldite 2015, AV138/HV998, and FM73. The results indicated that AV138/HV998 yielded the lowest SIF, followed by Araldite 2015, with FM73 producing the highest SIF as evident in Figure 23. This outcome can be explained by considering both the mechanical and thermal properties of the adhesives. Under thermo-mechanical loading, the thermal expansion coefficient becomes a critical factor. AV138's intermediate thermal expansion coefficient of $67 \times 10^{-6}/°C$ provides a balance that minimizes stress concentrations due to thermal expansion and contraction. This property, combined with its mechanical attributes, results in the least SIF. Araldite 2015, while mechanically robust, has a higher thermal expansion

coefficient of $85 \times 10^{-6}/°C$, which likely causes greater thermal stresses, slightly reducing its effectiveness compared to AV138/HV998. FM73, with the lowest thermal expansion coefficient of $50 \times 10^{-6}/°C$, does not expand as much under temperature changes. However, its significantly lower Young's modulus and shear modulus make it less effective at stress mitigation, resulting in the highest SIF. Therefore, the combined influence of mechanical stiffness and thermal expansion properties of the adhesives under thermo-mechanical loading conditions explains the observed results, highlighting the importance of selecting adhesives with balanced properties for optimal repair performance.
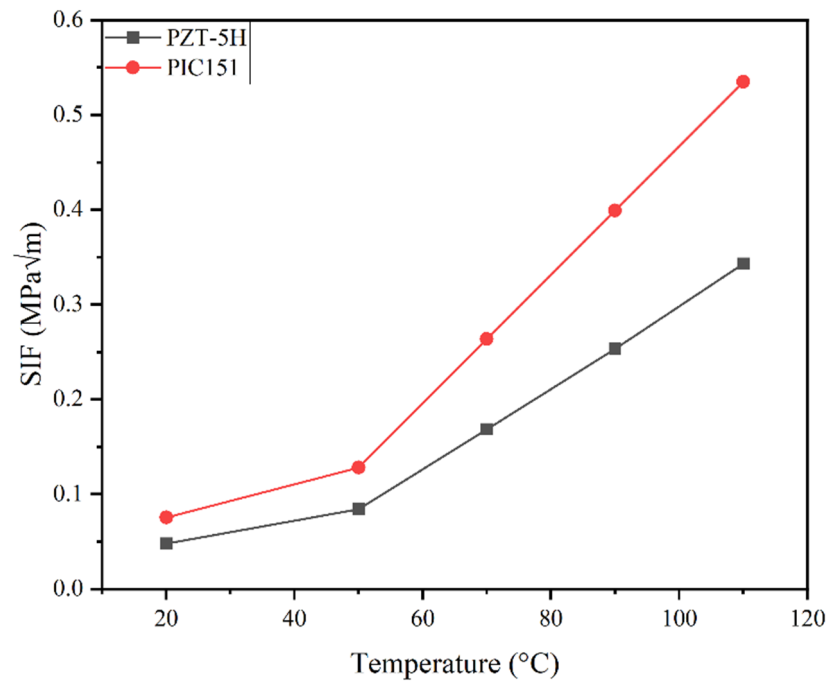

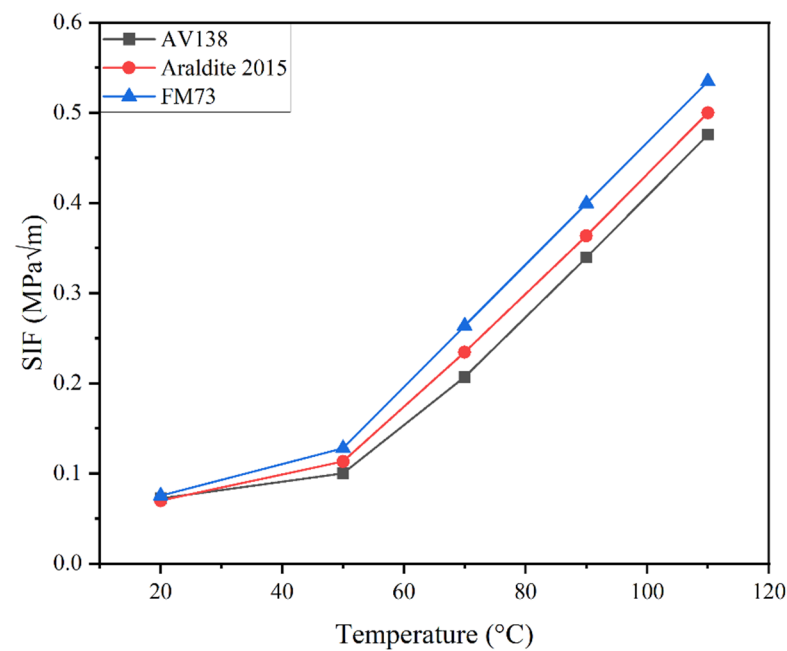**Figure 22.** SIF for different PZT materials under thermo-mechanical loading.

Figure 23. SIF for different adhesives under thermo-mechanical loading.

5.7.6. Effect of Adhesive Thickness

From Figure 24, it is evident that under thermo-mechanical loading, the SIF increased with an increase in adhesive thickness. This behaviour can be attributed to the combined effects of thermal and mechanical stresses in the system. The adhesive used in the repair has a relatively high coefficient of thermal expansion (CTE) of $50 \times 10^{-6}/°C$. As the adhesive layer thickness increases, the adhesive expands more significantly when subjected to temperature changes. This substantial thermal expansion can lead to increased mismatch stresses between the adhesive and the surrounding materials (such as the plate and the patch), exacerbating the stress concentrations at the crack tip. Additionally, the thicker adhesive layer's higher compliance under mechanical loads means that it deforms more easily, which reduces the effectiveness of load transfer and stress distribution from the patch to the plate. This decreased efficiency in transferring compressive stresses generated by actuation further lessens the patch's ability to mitigate the stress concentration at the crack tip. The combined effect of thermal expansion and mechanical compliance leads to an overall increase in SIF with thicker adhesive layers. Therefore, while thicker adhesives can improve adhesion strength, their higher thermal expansion and mechanical compliance under thermo-mechanical loading conditions necessitate careful optimization to ensure efficient load transmission and stress mitigation, maintaining the structural integrity of the repaired system.
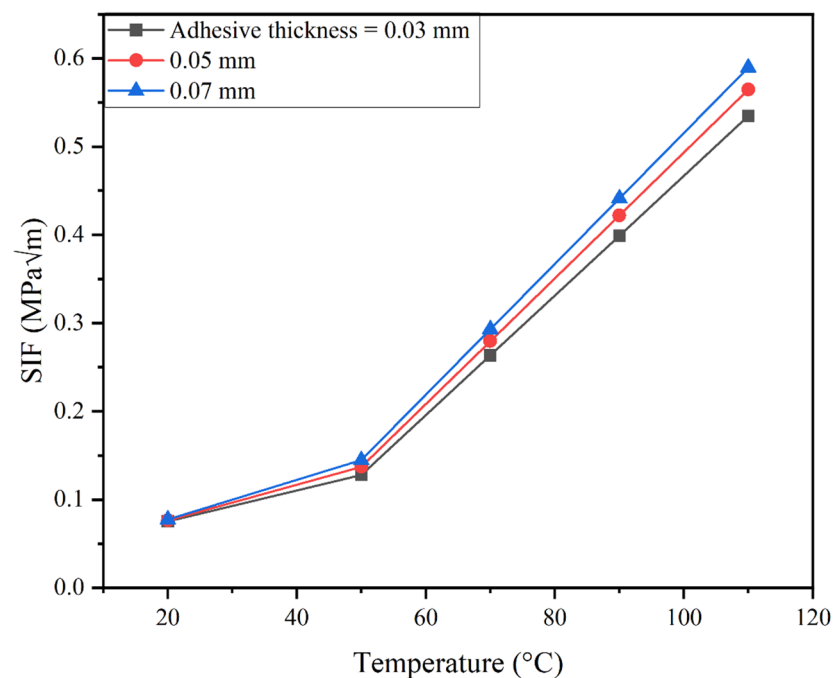

Figure 24. SIF for adhesive thicknesses under thermo-mechanical loading.

5.7.7. Effect of Increasing Applied Voltage

In the study of active repair using PZT patches under thermo-mechanical loading, the impact of increasing the applied voltage on the PZT patches was analyzed at a temperature of 110 °C. The results indicated a reduction in the SIF with increasing applied voltage, like the mechanical loading case. However, the reduction in SIF was only 14.7% when the voltage was increased from 0V to 140V as can be seen from Figure 25. This reduction is significantly less compared to the case under purely mechanical loading, where a 46% reduction in SIF was observed. The relatively smaller reduction in SIF under thermo-mechanical loading can be attributed to the combined effects of thermal expansion and mechanical loading on the crack tip stress field. The effectiveness of the PZT patches in reducing the SIF is diminished under thermo-mechanical loading because the thermal stresses induced by the differential expansion are significant and add to the overall stress

at the crack tip. The thermal expansion of the aluminium plate and adhesive is more pronounced due to their higher CTEs, leading to greater tensile stresses that the PZT patches must counteract. As a result, the compressive stresses generated by the PZT patches due to the applied voltage are less effective in reducing the overall stress intensity at the crack tip.
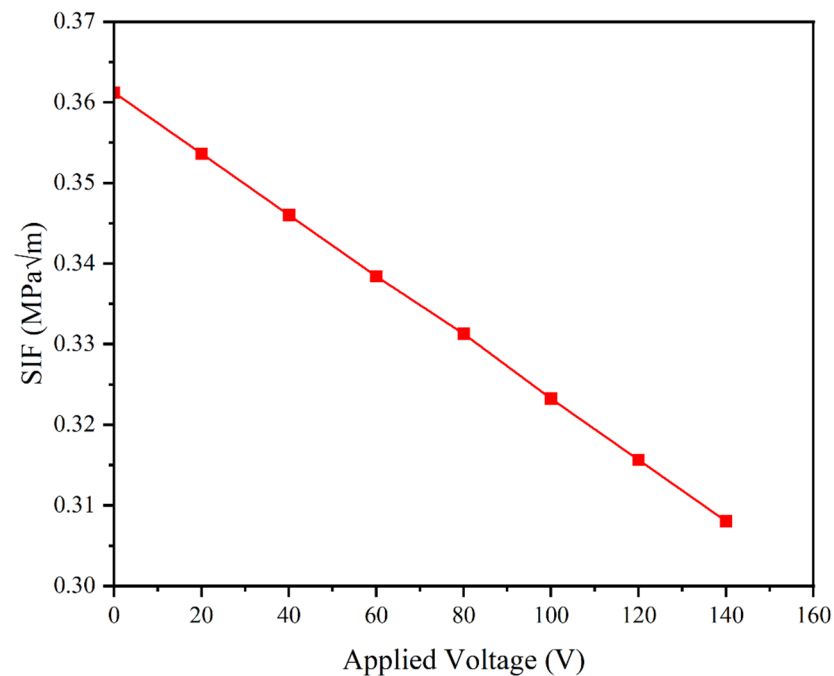

Figure 25. SIF for increasing applied voltage under thermo-mechanical loading.

5.8. Comparison of Mechanical and Thermo-Mechanical Loads

Figure 26 illustrates the variation in SIF with respect to crack length for a cracked plate actively repaired using PZT actuators. The results are presented for a purely mechanical loading condition (1 MPa) and combined thermo-mechanical loading conditions at temperatures of 50 °C, 70 °C, 90 °C, and 110 °C.

Under purely mechanical loading (1 MPa), the SIF exhibits a relatively gradual increase with increasing crack length. This indicates that the PZT actuators are effective in mitigating the stress concentration at the crack tip, thereby stabilizing the crack and preventing significant propagation. The trend shows a consistent but moderate rise in SIF, suggesting that the compressive stresses induced by the PZT actuators remain effective across different crack lengths, albeit with slightly reduced efficiency as the crack length increases. This behaviour is expected as longer cracks have larger surface areas and higher stress concentrations, which challenge the mitigation effects of the actuators.

In the presence of combined thermo-mechanical loading, a markedly different behaviour is observed. The SIF values are significantly higher across all crack lengths when thermal loads are introduced. At 50 °C, the SIF shows a 51% increase compared to the purely mechanical loading condition. This trend continues with increasing temperature, showing a 111% increase at 70 °C, 136% at 90 °C, and 150% at 110 °C. This dramatic increase in SIF with temperature can be attributed to the differential thermal expansion between the PZT patch, the host plate, and the adhesive layer. As temperature rises, the host plate, with its higher CTE, expands more than the PZT patch. The adhesive layer, having an even higher CTE, exacerbates this mismatch by expanding the most. These differential expansions induce significant thermal stresses at the crack tip, which add to the mechanical stresses already present.

The graph clearly shows that the SIF increases not only with crack length but also with temperature, indicating that the thermal stresses dominate and amplify the stress intensity

at the crack tip. This is particularly evident at higher temperatures, where the induced thermal stresses become substantial enough to significantly overshadow the compressive stresses generated by the PZT actuators. Consequently, the effectiveness of the PZT patches in reducing the SIF diminishes with increasing temperature.
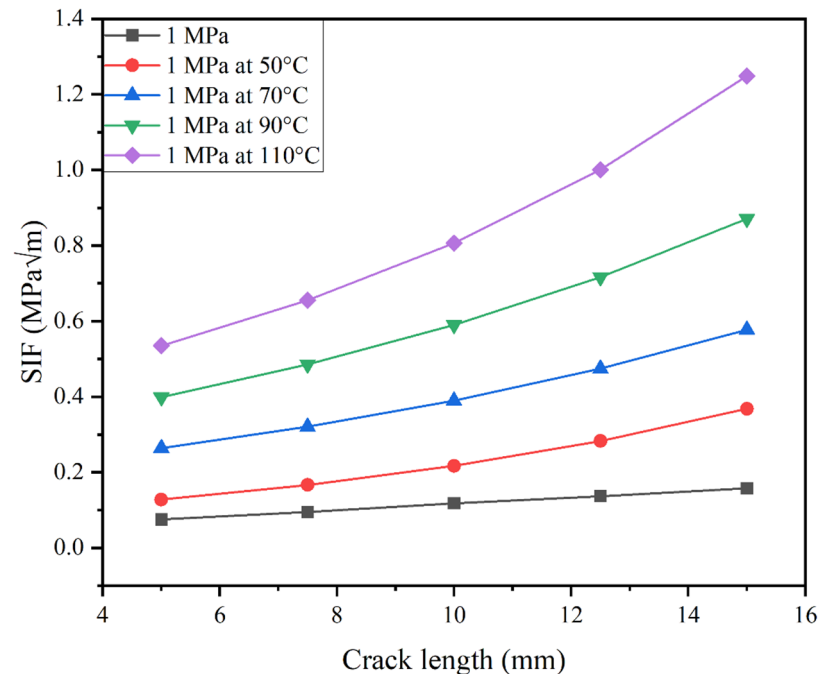

Figure 26. Comparison of SIF under mechanical and thermo-mechanical loading.

The comparative analysis reveals that while PZT actuators are effective in reducing SIF under mechanical loading, their effectiveness is considerably reduced under thermo-mechanical loading. The sharp increase in SIF with temperature highlights the challenges of maintaining effective crack mitigation in environments where thermal loads are present. The increased SIF with both temperature and crack length suggests that the thermal mismatch between different materials plays a critical role in stress concentration at the crack tip. The findings emphasize the necessity for considering thermal effects in the design and analysis of PZT actuator-based repair systems, especially for applications involving high temperatures. It also suggests that additional measures, such as optimizing the material properties of the PZT patch and adhesive or incorporating thermal barrier coatings, may be required to enhance the effectiveness of the active repair in thermo-mechanical environments.

6. Conclusions

This study provided a comprehensive analysis of the impact of thermal loading on the repair performance of cracked plates using PZT patches, revealing significant insights into the variations in SIF under different loading conditions and parameter configurations. The results demonstrated that SIF increases notably with both positive and negative temperature variations, highlighting the significant effect of thermo-mechanical loading on crack propagation. Thinner PZT patches were found to yield lower SIF values under mechanical loading, whereas thicker patches proved more effective under thermo-mechanical loading, indicating a complex relationship between patch thickness and loading conditions. Among the materials tested, PZT-5H consistently showed superior performance, maintaining lower SIF values in both scenarios, which underscores its robustness and versatility. Adhesive choice was also critical; Araldite 2015 was most effective under mechanical loading, while AV138/HV998 excelled under thermo-mechanical conditions due to its balanced mechanical and thermal properties. Increased adhesive thickness led to higher

SIF values across both loading conditions, emphasizing the need for precise adhesive application. Additionally, while increased applied voltage reduced SIF under mechanical loading, its effectiveness decreased under thermo-mechanical conditions, suggesting that parameter adjustments must be carefully calibrated. These findings offer valuable guidance for improving structural repair practises and set the stage for future advancements in engineering maintenance.

Author Contributions: Conceptualization, M.A.; methodology, M.A., M.H. and A.A.; software, M.A.; validation, M.A., M.H. and A.A.; investigation, M.A.; resources, M.A., M.H. and N.A.A.; writing— original draft, M.A.; writing—review and editing, M.A., M.H. and A.A.; funding acquisition, M.H., A.A. and M.B.; supervision, M.H., A.A. and N.A.A. All authors have read and agreed to the published version of the manuscript.

Data Availability Statement: The original contributions presented in the study are included in the article; further inquiries can be directed to the corresponding author/s.

Conflicts of Interest: The authors declare no conflicts of interest.

Notation and Abbreviations

a	crack length
SIF	stress intensity factor
K_I	mode I stress intensity factor
σ	stress
V	applied piezoelectric voltage
E	Young's modulus
CTE	thermal expansion coefficient
ΔT	change in temperature
σ_{xx}	normal stress in x-direction
σ_{yy}	normal stress in y-direction
τ_{xy}	shear stress
r	radial distance from crack tip
θ	angular coordinate around the crack tip
Δv	displacement of one crack face relative to the other
μ	shear modulus
k	dimensionless correction factor
LEFM	linear elastic fracture mechanics
3D	three dimensional
G	energy release rate

References

1. Crawley, E.F.; De Luisj, J. Use of Piezoelectric Actuators as Elements of Intelligent Structures. *AIAA J.* **1987**, *25*, 1373–1385. [CrossRef]
2. Abuzaid, A.; Hrairi, M.; Dawood, M.S.I.S. Survey of active structural control and repair using piezoelectric patches. *Actuators* **2015**, *4*, 77–98. [CrossRef]
3. Aabid, A.; Hrairi, M.; Mohamed Ali, S.J.; Ibrahim, Y.E. Review of Piezoelectric Actuator Applications in Damaged Structures: Challenges and Opportunities. *ACS Omega* **2022**, *8*, 2844–2860. [CrossRef] [PubMed]
4. Abuzaid, A.; Hrairi, M.; Dawood, M.S. Experimental and numerical analysis of piezoelectric active repair of edge-cracked plate. *J. Intell. Mater. Syst. Struct.* **2018**, *29*, 3656–3666. [CrossRef]
5. Ju, M.; Dou, Z.; Li, J.W.; Qiu, X.; Shen, B.; Zhang, D.; Yao, F.Z.; Gong, W.; Wang, K. Piezoelectric Materials and Sensors for Structural Health Monitoring: Fundamental Aspects, Current Status, and Future Perspectives. *Sensors* **2023**, *23*, 543. [CrossRef]

6.   Wang, Q.; Quek, S.T. Repair of delaminated beams via piezoelectric patches. *Smart Mater. Struct.* **2004**, *13*, 1222–1229. [CrossRef]
7.   Aabid, A.; Raheman, M.A.; Ibrahim, Y.E.; Anjum, A.; Hrairi, M.; Parveez, B.; Parveen, N.; Mohammed Zayan, J. A systematic review of piezoelectric materials and energy harvesters for industrial applications. *Sensors* **2021**, *21*, 4145. [CrossRef]
8.   Wang, Q.; Quek, S.T. Repair of cracked column under axially compressive load via piezoelectric patch. *Comput. Struct.* **2005**, *83*, 1355–1363. [CrossRef]
9.   Providakis, C.P. Repair of Cracked Structures under Dynamic Load Using Electromechanical Admittance Approach. *Key Eng. Mater.* **2007**, *348–349*, 49–52. [CrossRef]
10. Duan, W.H.; Quek, S.T.; Wang, Q. Finite element analysis of the piezoelectric-based repair of a delaminated beam. *Smart Mater. Struct.* **2008**, *17*, 015017. [CrossRef]
11. Wu, N.; Wang, Q. Repair of a delaminated plate under static loading with piezoelectric patches. *Smart Mater. Struct.* **2010**, *19*, 105025. [CrossRef]
12. Wu, N.; Wang, Q. An experimental study on the repair of a notched beam subjected to dynamic loading with piezoelectric patches. *Smart Mater. Struct.* **2011**, *20*, 115023. [CrossRef]
13. Platz, R.; Stapp, C.; Hanselka, H. Statistical approach to evaluating reduction of active crack propagation in aluminum panels with piezoelectric actuator patches. *Smart Mater. Struct.* **2011**, *20*, 085009. [CrossRef]
14. Alaimo, A.; Milazzo, A.; Orlando, C. On the dynamic behavior of piezoelectric active repair by the boundary element method. *J. Intell. Mater. Syst. Struct.* **2011**, *22*, 2137–2146. [CrossRef]
15. Abuzaid, A.; Hrairi, M.; Dawood, M.S. Mode I Stress Intensity Factor for a Cracked Plate with an Integrated Piezoelectric Actuator. *Adv. Mater. Res.* **2015**, *1115*, 517–522. [CrossRef]
16. Abuzaid, A.; Dawood, M.S.; Hrairi, M. Effects of Adhesive Bond on Active Repair of Aluminium Plate Using Piezoelectric Patch. *Appl. Mech. Mater.* **2015**, *799–800*, 788–793. [CrossRef]
17. Abuzaid, A.; Hrairi, M.; Dawood, M.S.I.S. Modeling approach to evaluating reduction in stress intensity factor in center-cracked plate with piezoelectric actuator patches. *J. Intell. Mater. Syst. Struct.* **2017**, *28*, 1334–1345. [CrossRef]
18. Abuzaid, A.; Hrairi, M.; Dawood, M.S.I.B.S. Evaluating the reduction of stress intensity factor in center-cracked plates using piezoelectric actuators. *Actuators* **2018**, *7*, 25. [CrossRef]
19. Jafari Fesharaki, J.; Madani, S.G.; Golabi, S. Best pattern for placement of piezoelectric actuators in classical plate to reduce stress concentration using PSO algorithm. *Mech. Adv. Mater. Struct.* **2020**, *27*, 141–151. [CrossRef]
20. Kumar, R.; Singh, A.; Tiwari, M. Investigation of Crack Repair in Orthotropic Composite by Piezoelectric Patching. 2020. Available online: https://www.sciencedirect.com/journal/materials-today-proceedings/vol/21/part/P2 (accessed on 16 February 2023).
21. Hai, T.T. Static repair of multiple cracked beam using piezoelectric patches. *Vietnam J. Mech.* **2021**, *43*, 197–207. [CrossRef]
22. Anjum, A.; Shaikh, A.A.; Hriari, M. Analysis of damage control of thin plate with piezoelectric actuators using finite element and machine learning approach. *Frat. Integrità Strutt.* **2023**, *66*, 112–126. [CrossRef]
23. Abdulla, M.; Hrairi, M.; Aabid, A.; Abdullah, N.A. Finite Element Analysis of a Repaired Cracked Aluminium Plate with Piezoelectric Patches under Mechanical and Thermal Loading. *J. Adv. Res. Appl. Sci. Eng. Technol.* **2024**, *51*, 171–183. [CrossRef]
24. Pattanayak, S.; Pohit, G. Reduction in Mode-I SIF of an Edge Cracked C-Shaped Specimen Using Piezoelectric Actuator. *E3S Web Conf.* **2023**, *430*, 01293. [CrossRef]
25. Shaikh, A.A.; Hriari, M.; Ali, J.S.M. Optimization of damage repair with piezoelectric actuators using the Taguchi method. *Frat. Ed Integrità Strutt.* **2024**, *67*, 137–152. [CrossRef]
26. Agrawal, B.N.; Treanor, K.E. Shape control of a beam using piezoelectric actuators. *Smart Mater. Struct* **1999**, *8*, 729–739. [CrossRef]
27. Kumar, R.; Singh, A.; Tiwari, M. Investigation of crack repair using piezoelectric material under thermo-mechanical loading. *J. Intell. Mater. Syst. Struct.* **2020**, *31*, 2243–2260. [CrossRef]
28. Voutetaki, M.E.; Providakis, C.P.; Chalioris, C.E. FRP Debonding Prevention of Strengthened Concrete Members under Dynamic Load using Smart Piezoelectric Materials (PZT). In Proceedings of the 15th European Conference on Composite Materials (ECCM15), Venice, Italy, 24–28 June 2012; p. 2170.
29. Hassani, S.; Mousavi, M.; Gandomi, A.H. Structural Health Monitoring in Composite Structures: A Comprehensive Review. *Sensors* **2022**, *22*, 153. [CrossRef]
30. Safian, A.; Soleimani, A. Piezoelectric Energy Harvesting from Direct Buoyancy Force. In Proceedings of the 3rd International Conference on Mechanical and Aerospace Engineering, Tehran, Iran, 24–26 April 2018; Available online: www.mechaero.ir (accessed on 29 March 2023).
31. Kumar, P. *Elements of Fracture Mechanics*; McGraw-Hill Education LLC: New York, NY, USA, 2010; Volume 70, ISBN 9780070656963.
32. Barsoum, R.S. Triangular quarter-point elements as elastic and perfectly-plastic crack tip elements. *Int. J. Numer. Methods Eng.* **1977**, *11*, 85–98. [CrossRef]
33. Barsoum, R.S. Application of quadratic isoparametric finite elements in linear fracture mechanics. *Int. J. Fract.* **1974**, *10*, 603–605. [CrossRef]
34. Henshell, R.D.; Shaw, K.G. Crack tip finite elements are unnecessary. *Int. J. Numer. Methods Eng.* **1975**, *9*, 495–507. [CrossRef]
35. Tada, H.; Paris, P.C.; Irwin, G.R. *Stress Analysis of Cracks Handbook Excerpts*; ASME Press: New York, NY, USA, 2000; pp. 40–47.
36. Lei, Y.; O'Dowd, N.P.; Webster, G.A. Fracture mechanics analysis of a crack in a residual stress field. *Int. J. Fract.* **2000**, *106*, 195–216. [CrossRef]
37. Canonsburg, T.D. ANSYS Mechanical APDL Verification Manual. *Knowl. Creat. Diffus. Util.* **2012**, *15317*, 724–746.

38.   Callister, W.D.; Rethwisch, D.G. Materials science and engineering. *Mater. Sci. Eng. A* **1980**, *42*, 181.
39.   Anderson, T.L. *Fracture Mechanics: Fundamentals and Applications*, 3rd ed.; CRC press: Boca Raton, FL, USA, 2005. [CrossRef]
40.   ANSYS. *ANSYS Element Reference Guide, Rev.2*; ANSYS: Canonsburg, PA, USA, 2022; Volume 22.